

## Discovery of a Novel L-Lyxonate Degradation Pathway in *Pseudomonas aeruginosa* PAO1

Salehe Ghasempur,<sup>†,§</sup> Subramaniam Eswaramoorthy,<sup>⊥</sup> Brandan S. Hillerich,<sup>||</sup> Ronald D. Seidel,<sup>||</sup> Subramanyam Swaminathan,<sup>⊥</sup> Steven C. Almo,<sup>||</sup> and John A. Gerlt\*,<sup>†,‡,§</sup>

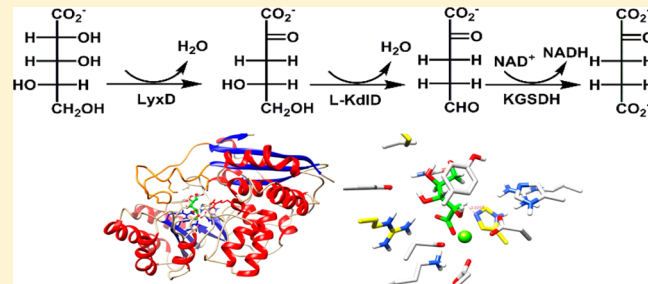
<sup>†</sup>Department of Biochemistry, <sup>‡</sup>Department of Chemistry, and <sup>§</sup>Institute for Genomic Biology, University of Illinois at Urbana–Champaign, 600 South Mathews Avenue, Urbana, Illinois 61801, United States

<sup>||</sup>Department of Biochemistry, Albert Einstein College of Medicine, 1300 Morris Park Avenue, Bronx, New York 10461, United States

<sup>⊥</sup>Biosciences Department, Brookhaven National Laboratory, Upton, New York 11973, United States

### Supporting Information

**ABSTRACT:** The L-lyxonate dehydratase (LyxD) *in vitro* enzymatic activity and *in vivo* metabolic function were assigned to members of an isofunctional family within the mandelate racemase (MR) subgroup of the enolase superfamily. This study combined *in vitro* and *in vivo* data to confirm that the dehydration of L-lyxonate is the biological role of the members of this family. *In vitro* kinetic experiments revealed catalytic efficiencies of  $\sim 10^4 \text{ M}^{-1} \text{ s}^{-1}$  as previously observed for members of other families in the MR subgroup. Growth studies revealed that L-lyxonate is a carbon source for *Pseudomonas aeruginosa* PAO1; transcriptomics using qRT-PCR established that the gene encoding LyxD as well as several other conserved proximal genes were upregulated in cells grown on L-lyxonate. The proximal genes were shown to be involved in a pathway for the degradation of L-lyxonate, in which the first step is dehydration by LyxD followed by dehydration of the 2-keto-3-deoxy-L-lyxonate product by 2-keto-3-deoxy-L-lyxonate dehydratase to yield  $\alpha$ -ketoglutarate semialdehyde. In the final step,  $\alpha$ -ketoglutarate semialdehyde is oxidized by a dehydrogenase to  $\alpha$ -ketoglutarate, an intermediate in the citric acid cycle. An X-ray structure for the LyxD from *Labrenzia aggregata* IAM 12614 with Mg<sup>2+</sup> in the active site was determined that confirmed the expectation based on sequence alignments that LyxDs possess a conserved catalytic His-Asp dyad at the end of seventh and sixth  $\beta$ -strands of the  $(\beta/\alpha)_7\beta$ -barrel domain as well as a conserved KxR motif at the end of second  $\beta$ -strand; substitutions for His 316 or Arg 179 inactivated the enzyme. This is the first example of both the LyxD function in the enolase superfamily and a pathway for the catabolism of L-lyxonate.



The number of sequences in the UniProtKB/TrEMBL and UniProtKB/SwissProt databases is increasing exponentially, with  $>54$  million nonredundant entries as of March 2014 (Release 2014\_03). However, the functions of less than 1% of these proteins have been experimentally characterized (UniProtKB/SwissProt). Most of the annotations in the sequence databases are based on automated methods that transfer the function from the “closest” homologue; however, this procedure is unreliable.<sup>1</sup> Given the number of proteins with unknown functions, conducting biochemical and genetic experiments for each protein individually is unrealistic.<sup>1,2</sup>

Characterization of an *in vitro* activity has been considered to be sufficient to assign biological function to an uncharacterized (unknown) enzyme. However, with the recognition that enzymes often are promiscuous *in vitro* and that this promiscuity may be irrelevant *in vivo*, *in vivo* evidence is necessary to confirm the *in vitro* activity as well as establish the *in vivo* metabolic/physiological function. For enzymes that function in metabolic pathways, characterization of the pathway in which the enzyme participates facilitates the assignment of both the correct *in vitro* activity as well as the physiological role of the enzyme.

This laboratory has been interested in understanding the structural basis for divergent evolution of function in the enolase superfamily, with the name reflecting the most abundant member of the superfamily. Functional assignment in the enolase superfamily provides a paradigm for the challenges faced in assigning functions to unknown enzymes discovered in genome projects: sequence homology alone is insufficient to transfer functional annotations from previously characterized members. For example, the majority of members of the mandelate racemase (MR) subgroup within the enolase superfamily catalyze the dehydration of acid sugars in catabolic pathways,<sup>3,4</sup> although the substrate specificities of these are unknown.

Members of the enolase superfamily share two conserved characteristics: an initial partial reaction and a structural scaffold. To date, all characterized members catalyze functionally diverse reactions initiated by abstraction of the proton of a carbon

Received: April 8, 2014

Revised: May 5, 2014

Published: May 6, 2014

located  $\alpha$  to a carboxylate group to form an enolate anion intermediate. For the proton abstraction to be kinetically competent, the intermediate is stabilized by coordination to a required  $Mg^{2+}$  ion. The intermediate then can undergo different fates such as the elimination of water or ammonia, cycloisomerization, epimerization, or racemization.<sup>5</sup>

Also, all structurally characterized members contain an N-terminal ( $\alpha + \beta$ ) capping domain that determines the substrate specificity and a C-terminal ( $\beta/\alpha$ )- $\beta$ -barrel domain (a modified TIM-barrel domain) that contains the residues required for catalysis. The active site is located at the interface between the capping and barrel domains. The barrel domain contains three carboxylate ligands for the required  $Mg^{2+}$  located at the ends of third, fourth, and fifth  $\beta$ -strands and conserved acid/base catalysts located at the C-terminal ends of the second, sixth, and/or seventh  $\beta$ -strands.<sup>6</sup> The identities and positions of these catalytic residues provide the ability to catalyze different reactions using the same structural scaffold. The identities and locations of the metal ion binding ligands and acid/base catalysts allows the superfamily to be partitioned into seven subgroups. The conserved metal binding and catalytic residues of the subgroups are presented in Supporting Information, Table 1. The MR subgroup is one of the largest subgroups, with a conserved His-Asp dyad located at the ends of the seventh and sixth  $\beta$ -strands functioning as an acid/base catalyst.

In this article, we report the L-lyxonate dehydratase (LyxD) function, a novel *in vitro* activity for a previously uncharacterized member of the MR subgroup, and the pathway in which LyxD participates to allow L-lyxonate to be used as a carbon source.

## MATERIALS AND METHODS

**Screen for Dehydration Activity.** Enzymes were screened for acid sugar dehydration activity with a library of 77 mono- and di-acid sugars using the semicarbazide assay.<sup>3</sup> The reaction solutions contained 50 mM Tris-HCl at pH 8.0, 5 mM  $MgCl_2$ , 1 mM acid sugar, and 1  $\mu M$  enzyme. The reactions (50  $\mu L$ ) were performed in Corning 96-well UV-transparent plates and were incubated at 30 °C for 16 h. A 250  $\mu L$  aliquot of a 1% semicarbazide solution in 1% sodium acetate was added; after incubation at room temperature for 1 h, the absorbance was measured at 250 nm with a TECAN microplate reader ( $\epsilon = 10,200 \text{ cm}^{-1} \text{ M}^{-1}$ ).

**Kinetic Assays of L-Lyxonate Pathway Enzymes.** LyxD activity was quantitated using a continuous enzyme-coupled spectroscopic assay. The 200  $\mu L$  mixture reaction contained 20 mM HEPES buffer at pH 7.5, 5 mM  $MgCl_2$ , 0.16 mM  $NAD^+$ , 0.025 mM to 1 mM L-lyxonate, 3  $\mu M$  2-keto-3-deoxy-L-lyxonate dehydratase (L-Kdl dehydratase), 3  $\mu M$   $\alpha$ -ketoglutarate semi-aldehyde dehydrogenase ( $\alpha$ KGSDH), and 21 nM LyxD. The reduction of  $NAD^+$  was monitored by the increase in absorbance at 340 nm ( $\epsilon = 6220 \text{ M}^{-1} \text{ cm}^{-1}$ ) with a PerkinElmer Lambda-14 UV-vis spectrophotometer.

Assays for the two pathway proteins L-Kdl dehydratase and  $\alpha$ KGSDH were similarly performed: the 200  $\mu L$  mixture reaction contained 20 mM HEPES buffer at pH 7.5, 5 mM  $MgCl_2$ , 0.16 mM  $NAD^+$ , 0.025 mM to 1 mM L-lyxonate, and 3  $\mu M$  L-lyxonate dehydratase. However, for the L-Kdl dehydratase assay 3  $\mu M$   $\alpha$ KGSDH and 21 nM L-Kdl dehydratase were added, and the reduction of  $NAD^+$  at 340 nm was measured. For the  $\alpha$ KGSDH assay, 21 nM  $\alpha$ KGSDH and 3  $\mu M$  L-Kdl dehydratase were added. These conditions provided a limiting amount of the assayed enzyme and an excess amount of the coupling enzyme in the reactions.

**Cloning, Expression, and Protein Purification.** The genes encoding L-Kdl dehydratase (UniProt ID Q9I1Q1) and  $\alpha$ KGSDH (UniProt ID Q9I1Q0) were PCR-amplified from *Pseudomonas aeruginosa* PAO1 ATCC 47085 genomic DNA. The 100  $\mu L$  reactions contained 1 ng of DNA, 20  $\mu L$  of 5× Phusion HF buffer, 0.2 mM dNTP, 1  $\mu L$  of NEB Phusion enzyme, and 40 pmol primers complementary to the beginning and end of the genes containing desired restriction enzyme sites and used a PTC-200 Gradient thermocycler. The digested PCR products were ligated into the pET-1Sb vector linearized with the same restriction enzymes. The ligation product was transformed in XL1Blue electrocompetent cells.

The proteins were expressed in *E. coli* BL21 (DE3) cells transformed with expression plasmids grown at 37 °C in the presence of 100  $\mu g/mL$  ampicillin until  $OD_{600} = 0.5$ , at which point the cells were induced by the addition of 1 mM IPTG; growth was continued overnight. The cells were harvested by centrifugation (15 min at 4500g), resuspended in binding buffer (5 mM imidazole, 0.5 M NaCl, 5 mM  $MgCl_2$ , and 20 mM Tris-HCl at pH 7.9), lysed by sonication, and clarified by centrifugation. The lysate containing the His-tagged protein was loaded on a 5 mL HisTrap FF crude column (GE Healthcare) equilibrated with binding buffer and eluted with a linear 80 mL gradient from 0% to 100% of elution buffer (1 M imidazole, 0.5 M NaCl, and 20 mM Tris-HCl at pH 7.9).

The expression  $\alpha$ KGSDH yielded soluble His-tagged protein, which was purified by a  $Ni^{2+}$  column as mentioned above. L-Kdl dehydratase was not soluble with the His-tag; however, it was soluble when purified using the pMAL-c2X plasmid containing maltose binding protein (MBP-Tag). The protein was loaded on MBP Trap HP (GE Healthcare) and eluted with MBP elution buffer (20 mM HEPES at pH 7.5, 100 mM KCl, and 10 mM maltose).

The gene encoding the LyxD from *Labrenzia aggregata* IAM 12614 (UniProt ID A0NP48) was cloned into expression vector pNIC28-BSA4 by PCR and the ligation-independent cloning method as previously described.<sup>7</sup> The resulting plasmid was transformed into BL21(DE3) *E. coli* containing the pRIL plasmid (Stratagene) and used to inoculate a 20 mL 2xYT culture containing 50  $\mu g/mL$  kanamycin and 34  $\mu g/mL$  chloramphenicol. The culture was allowed to grow overnight at 37 °C in a shaking incubator. The overnight culture was used to inoculate 2 L of ZYP-5052 autoinduction media (Studier). The expression culture was placed in a LEX48 airlift fermenter and incubated at 37 °C for 4 h and then at 22 °C overnight (16–20 h). The culture was harvested, pelleted by centrifugation at 6000g for 10 min, and stored at –80 °C.

The cells were resuspended in lysis buffer (20 mM HEPES at pH 7.5, 20 mM imidazole, 500 mM NaCl, 5% glycerol, and 5 mM  $MgCl_2$ ) and lysed by sonication. The lysate was clarified by centrifugation at 35,000g for 45 min. The clarified lysate was loaded onto a 1 mL HisTrap Ni-NTA column (GE Healthcare) using an AKTAexpress FPLC (GE Healthcare), washed with 10 column volumes of lysis buffer, and eluted in buffer containing 20 mM HEPES at pH 7.5, 500 mM NaCl, 500 mM imidazole, 5% glycerol, and 5 mM  $MgCl_2$ . The purified sample was loaded onto a HiLoad S200 16/60 PR gel filtration column equilibrated with buffer containing 20 mM HEPES at pH 7.5, 150 mM NaCl, 5% glycerol, 5 mM  $MgCl_2$ , and 5 mM DTT. The purity of the protein was analyzed by SDS-PAGE, snap frozen in liquid nitrogen, and stored at –80 °C.<sup>8</sup>

**Site-Directed Mutagenesis.** Site-directed mutants were generated using the overlap extension method.<sup>9</sup> PCR reactions

(50  $\mu$ L) containing 1 ng of plasmid encoding wild-type L-lyxonate dehydratase, 5  $\mu$ L of 10 $\times$  PCR buffer, 4 mM MgCl<sub>2</sub>, 2 mM dNTPs, 40 pmol of each primer, and 0.5 units of Phusion (NEB) were performed to yield megaprimer. The 3'-megaprimer was constructed using the T7term primer and a sense primer encoding the desired mutation. The 5'-megaprimer was constructed using the T7pro primer and an antisense primer encoding the desired mutation. The PCR cycle was as follows: 95 °C for 4 min followed by 26 cycles of 95 °C for 45 s, 55 °C for 45 s, and 72 °C for 2 min and 15 s, followed by 7 min at 72 °C. The primers were purified by 1% agarose gel electrophoresis followed by gel extraction (Qiagen). The second reaction mixture (50  $\mu$ L) contained 5  $\mu$ L of 10 $\times$  PCR buffer, 4 mM MgCl<sub>2</sub>, 2 mM dNTPs, 40 pmol each of T7pro and T7term, 200 pmol of each megaprimer, and 1 unit of Phusion enzyme. The PCR cycle described above was utilized for this reaction. The mutant fragments were digested with XbaI (NEB) and NdeI (NEB) and cloned into the pET-15b vector. The plasmids were sequenced to confirm the presence of the expected mutations.

**Growth Experiments.** Luria–Bertani broth (LB) cultures (4 mL) of single colonies were grown overnight. Then, the cultures were washed three times with 0.5 mL of M9 minimal medium (6.78 g/L Na<sub>2</sub>HPO<sub>4</sub> 7H<sub>2</sub>O, 3 g/L KH<sub>2</sub>PO<sub>4</sub>, 1 g/L NH<sub>4</sub>Cl, and 0.5 g/L NaCl). The cells were resuspended in M9 medium and then used to inoculate fresh 4 mL glucose M9 minimal media cultures to a starting OD<sub>600</sub> of 0.05. The cultures were grown to OD<sub>600</sub> of 0.4; then, the cells were washed three times in M9 minimal medium. The washed cells were used to inoculate 300  $\mu$ L of the M9 medium containing a library of aldoses and aldonates in a Honeycomb 2 plate. The experiments were performed at 37 °C using a Bioscreen-C automated growth curve analysis system measuring absorbance at 600 nm every 20 min.

**qRT-PCR. *Pseudomonas aeruginosa*.** PAO1 ATCC 47085 was grown in 5 mL of 0.4% glucose M9 minimal medium. The cells were harvested and washed 3 times with M9 minimal medium. The cells were used to inoculate two 5 mL cultures of M9 minimal medium, one containing 0.4% L-lyxonate, and the second 0.4% glucose. Both cultures were grown to a final cell density OD<sub>600</sub> of 0.1. Then cells were grown aerobically at 37 °C to an OD<sub>600</sub> of 0.5. For preparation of RNA, an equal volume of RNAProtect bacteria reagent (Qiagen) was added to each culture. After 5 min, the cells were harvested (10,000g for 5 min at 4 °C); RNA was isolated from the cells using an RNeasy Mini Kit (Qiagen) following the manufacturer's protocols. The isolated RNA was quantitated by measuring the absorbance at 260 nm, with one OD corresponding to 44  $\mu$ g mL<sup>-1</sup>. The purity and integrity of the RNA were assessed spectrophotometrically and with a 2% agarose gel.

Reverse transcription was performed on 1  $\mu$ g of RNA by using the RevertAid H Minus First Strand cDNA synthesis kit (Fermentas) according to the manufacturer's protocol. For each gene, 1  $\mu$ L of the resulting cDNA was PCR-amplified in 20  $\mu$ L of reaction mixture. Primers for each gene were designed by the Universal Pro-Be library system (Roche Applied Science). Real-time PCR was carried out in 96-well plates using a Roche LightCycler 480 (LC480). The 20  $\mu$ L PCR reaction was prepared by adding 1  $\mu$ L of cDNA template, 2  $\mu$ L each of 150 nM forward and reverse primers, and 10  $\mu$ L of SYBR 2 $\times$  the concentration of Green Master Mix (Roche). Also, real time PCR reactions with isolated RNA samples as template were performed to assess contamination by genomic DNA. The PCR conditions were 1 cycle at 95 °C for 5 min, 40 cycles of

amplification at 95 °C for 15 s, followed by 60 °C for 1 min. The efficiencies of the primers were calculated as 95 ± 2%. The gene expression data were expressed as Cp or cross-point value; the 16S rRNA gene was used as a reference. The data were analyzed by the 2<sup>-ΔΔCT</sup> calculation method<sup>10</sup> and are the averages of three biological replicates. Primer sequences are provided in Supporting Information, Table 2.

**Crystallization and Data Collection.** LyxD from *L. aggregata* IAM 12614 (UniProt ID A0NP48) was crystallized by the sitting drop vapor diffusion method using Hampton Research crystallization screens. The protein solution (0.5  $\mu$ L; 12 mg/mL) was mixed with an equal volume of reservoir solution and equilibrated against 100  $\mu$ L of the same reservoir solution at room temperature. Acceptable crystals were obtained using 0.5 M magnesium formate and 0.1 M Bis-Tris at pH 6.5 as precipitant. Crystals were mounted on cryoloops using 20% glycerol as the cryoprotectant and were flash-frozen in liquid nitrogen. X-ray diffraction data were collected at 100 K at beamline X29 of National Synchrotron Light Source, Brookhaven National Laboratory. The crystals belong to tetragonal space group I422 with the unit cell parameters  $a = b = 135.24$  and  $c = 116.73$  Å. Data collection statistics are presented in Table 1.

**Table 1. Data Collection and Refinement Statistics**

data collection	
space group	I422
unit cell parameters (Å, deg)	$a = b = 135.24$ and $c = 116.73$ $\alpha = \beta = \gamma = 90.0$
R-merge <sup>1</sup>	0.106 (0.155)
resolution (Å)	50.0–1.88 (1.91–1.88)
completeness (%)	100 (100)
number of unique reflections	44115 (2168)
redundancy	29.1 (28.7)
$I/\sigma(I)$	15.8
refinement	
resolution (Å)	44.19–1.88 (2.0–1.88)
completeness (%)	99.6 (99.4)
R-factor <sup>2</sup>	
R-work	0.166 (0.17)
R-free	0.185 (0.205)
number of reflections	
R-work	43953 (6838)
R-free	2194 (365)
RMS deviations	
bond lengths (Å)	0.005
bond angles (deg)	1.3
dihedral angle (deg)	22.4
improper angles (deg)	0.77
number of atoms	
protein	3075
solvent	238
Mg ion	1
Ramachandran plot	
most favorable	297 (89.5%)
additionally allowed	30 (9.0%)
generously allowed	2 (0.6%)
disallowed	3 (0.9%)

The diffraction data were processed and scaled using HKL2000 to generate a unique set of X-ray intensity data.<sup>11</sup> The structure was solved by the molecular replacement method

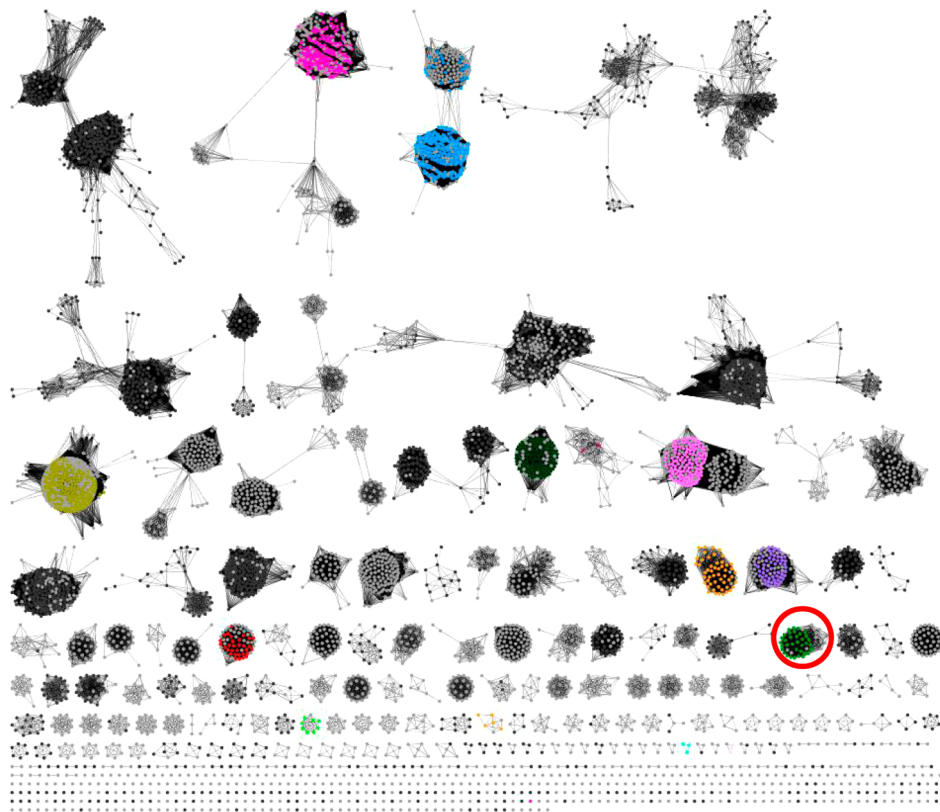


**Figure 1.** Representative node sequence similarity network for the enolase superfamily member excluding the enolase subgroup. Sequences are shown schematically as nodes (circles); BLAST connections with E-values  $\leq 10^{-85}$  are shown as edges (lines) that connect the nodes. At this E-value, sequences with known functions cluster together suggesting that the other clusters likely are isofunctional. Sequences that have unknown functions are colored gray. The circled cluster is the LyxD family.

using MOLREP (search model: 3SQS) and initially refined as a rigid body.<sup>12</sup> The initial model was used to generate phases, and the structure was rebuilt by ARP-wARP.<sup>13</sup> The model was refined in stages by CNS 1.1; the refinement parameters are included in Table 1.<sup>14</sup> Model evaluation, addition of water molecules, and fine adjustment of the final model were carried out with COOT.<sup>15</sup> Structure refinement converged with excellent geometrical parameters of bond lengths and angles. Model coordinates and structure factors have been deposited at the PDB (3STP). Because the protein sample was prepared in the presence of 5 mM MgCl<sub>2</sub> and crystallized with magnesium formate, a magnesium ion with six coordination sites was modeled in the active site.

## RESULTS AND DISCUSSION

**Sequence Similarity Network.** A representative node sequence similarity network for the acid sugar dehydratases in the enolase superfamily is shown in Figure 1 (MR, D-glucarate dehydratase, and D-mannonate dehydratase subgroups). This network was constructed using a BLAST e-value threshold of  $10^{-85}$  and collects all sequences sharing  $>95\%$  sequence identity into the same “metanode”. The circled cluster in Figure 1 represents the sequences that are the subject of this study. At this e-value threshold, the sequences in the various clusters share  $\sim 40\%$  sequence identity. Gray nodes represent proteins for which the *in vitro* activity is unknown; nodes that are colored have assigned *in vitro* activities.<sup>16</sup> To date, 9 different functions have been reported within the MR subgroup, MR, and 8 acid sugar dehydratases with different substrate specificities, including D-arabinonate dehydratase (AraD),<sup>17</sup> L-fuconate dehydratase

(FucD),<sup>3</sup> D-galactonate dehydratase (GalD),<sup>18</sup> D-tartrate dehydratase (TarD),<sup>19</sup> D-gluconate dehydratase (GlcD),<sup>20,21</sup> L-talarate/galactarate dehydratase (TalrD/GalrD),<sup>22</sup> L-galactonate dehydratase,<sup>23</sup> and L-rhamnonate dehydratase (RhamD).<sup>16</sup> Enzymes with novel substrate specificities/functions are expected to populate the gray clusters.

### Substrate Identification Using the Acid Sugar Library.

Two uncharacterized proteins, one from *Verminephrobacter eiseniae* (UniProt ID A1WLE4) and the second from *Dianorosibacter shabila* (UniProt ID A8LS88), were screened for dehydration activity on a library of di- and monoacid sugars using the semicarbazide assay.<sup>3</sup> After a 16 h incubation at 30 °C, both proteins quantitatively converted 1 mM L-lyxonate and 1 mM D-gulonate to their 2-keto-3-deoxy dehydration products; 1 mM L-mannonate was converted to its dehydration product with a 50% yield. The configurations of these three acid sugars are identical at carbons 2–4 (Scheme 1). The kinetic constants

### Scheme 1

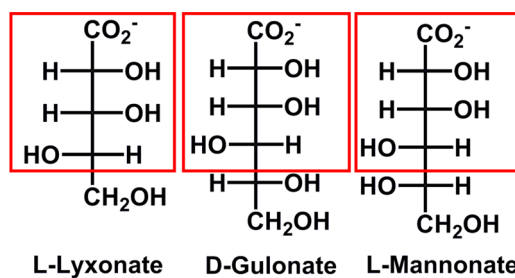


Table 2. Kinetic Constants for LyxD and Its Mutants

	enzyme	UniProt	substrate	$k_{cat}$ (s <sup>-1</sup> )	$K_m$ (mM)	$k_{cat}/K_m$ (M <sup>-1</sup> s <sup>-1</sup> )
(A)	LyxD-wild type	A1WLE4	L-lyxonate	3 ± 0.3	0.4 ± 0.1	8 × 10 <sup>3</sup>
			D-gulonate	2 ± 0.4	1 ± 0.2	2 × 10 <sup>3</sup>
			L-mannone	NA	NA	0.08
(B)	LyxD-wild type	A8LS88	L-lyxonate	2 ± 0.2	0.2 ± 0.05	1 × 10 <sup>4</sup>
			D-gulonate	3 ± 0.3	1 ± 0.3	3 × 10 <sup>3</sup>
			L-mannone	NA	NA	0.04
(B)	LyxD-Y216F	A8LS88	L-lyxonate	2 ± 0.3	0.2 ± 0.05	1 × 10 <sup>4</sup>
	LyxD-R179Q	A8LS88	L-lyxonate	NA	NA	0.01
	LyxD-R179 K	A8LS88	L-lyxonate	Ins <sup>a</sup>	Ins <sup>a</sup>	Ins <sup>a</sup>
	LyxD-H316Q	A8LS88	L-lyxonate	NA	NA	0.08

<sup>a</sup>Insoluble.

for the three substrates were determined for both enzymes using a coupled enzyme assay. Dehydration of L-lyxonate and D-gulonate occurred with values for  $k_{cat}/K_m$  of  $\sim 10^4$  M<sup>-1</sup> s<sup>-1</sup> (Table 2A); in contrast, dehydration of L-mannone occurred with low catalytic efficiency.

**Genome Neighborhood.** We used *Pseudomonas aeruginosa* PAO1 to determine the *in vivo* functions of these enzymes because (1) its genome is expected to encode an efficient LyxD (70% sequence identity with A1WLE4 and A8LS88; Table 2A; the specificity determining residues in the active site are conserved) and (2) the organism is genetically tractable. Using M9 minimal medium in the presence of 0.4% L-lyxonate, D-gulonate, or L-mannone, we observed growth only with L-lyxonate (Figure 2);

two kinetically characterized LyxD (UniProt IDs A1WLE4 and A8LS88). A plausible pathway for the catabolism of L-lyxonate is shown in Scheme 2. This pathway involves dehydration of the product of the LyxD-catalyzed reaction, 2-keto-3-deoxy-5R-hydroxypentanoate, also known as 2-keto-3-deoxy-L-lyxonate (L-Kdl) or 2-keto-3-deoxy-L-arabinonate (L-Kda), to generate  $\alpha$ -ketoglutarate semialdehyde ( $\alpha$ KGS) that is the substrate for a dehydrogenase that generates  $\alpha$ -ketoglutarate, an intermediate in the citric acid cycle. Candidate proteins to perform both of these functions are encoded by the genome neighborhood.

**Transcriptomics.** To investigate whether the genes that encode the LyxD and the putative L-Kdl dehydratase and  $\alpha$ KGS dehydrogenase are up-regulated when *P. aeruginosa* PAO1 is grown on L-lyxonate as carbon source, qRT-PCR was used to measure transcript levels relative to the level observed with D-glucose as carbon source (Supporting Information, Table 2). The genes encoding these putative enzymes in the L-lyxonate catabolic pathway as well as others in the genome neighborhood are upregulated 5- to 20-fold when L-lyxonate was used as the carbon source compared to growth on D-glucose (Figure 4). The up-regulated genes encode a member of the amidohydrolase (AH) superfamily (IPR006992), a member of the 4-hydroxy-threonine-4-phosphate dehydrogenase family (IPR005255; PdxA-like protein), LyxD (IPR001354), a member of the fumarylacetate hydrolase superfamily (IPR005255; the putative L-Kdl dehydratase), and a dehydrogenase (IPR016161; the putative  $\alpha$ KGS dehydrogenase;  $\alpha$ KGSDH).

We also used the cDNA generated from the RNA transcripts isolated when L-lyxonate was used as a carbon source to determine which genes are cotranscribed, with the expectation that these would participate in the same pathway. In Figure 3, the genes on the same transcript are designated with the same color: (1) green, a transporter, the member of the AH superfamily and the PdxA-like protein; (2) magenta, a second transporter, LyxD, and L-Kdl dehydratase; and (3) orange,  $\alpha$ KGSDH. These transcript assignments are in good agreement with the qRT-PCR results in which genes on the same transcript are equivalently up-regulated.

**Characterization of the Pathway Enzymes: L-Kdl Dehydratase.** To further explore the L-lyxonate catabolic pathway, the genes that were up-regulated in *P. aeruginosa* PAO1 were separately cloned into the pET-15b expression vector and overexpressed, and the proteins were purified to homogeneity. Unfortunately, the putative LyxD was expressed as an insoluble protein; however, because it shares 70% sequence identity with the kinetically characterized LyxDs and its active site contains the same substrate specificity determining residues (*vide infra*), we conclude that this protein is a LyxD.

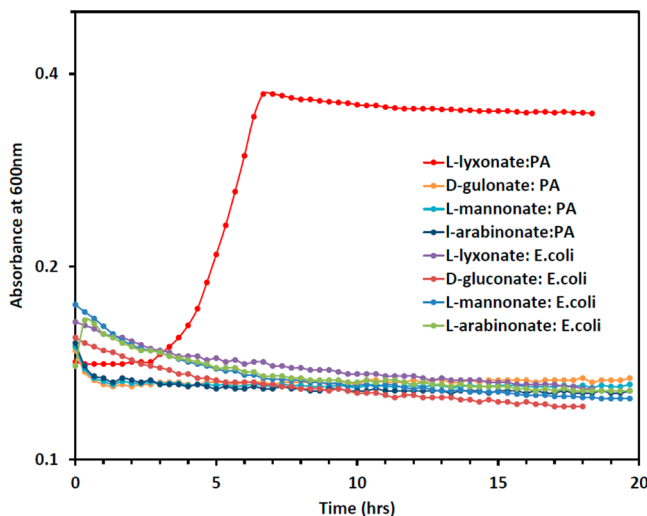
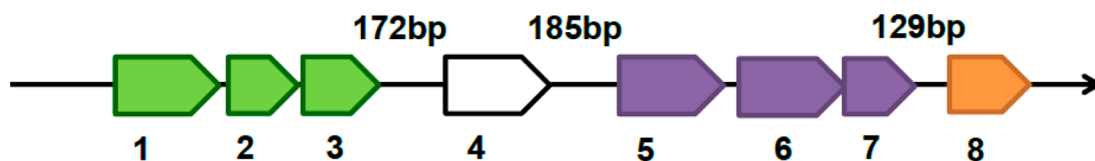


**Figure 2.** Growth screening of *Pseudomonas aeruginosa* PAO1. *P. aeruginosa* PAO1 can utilize L-lyxonate, D-gulonate, L-mannone, and L-arabinonate as the carbon source. *E. coli* is not able to metabolize L-lyxonate.

therefore, we conclude that *P. aeruginosa* PAO1 has a catabolic pathway for the utilization of L-lyxonate. In many sugar catabolic pathways, an aldose is oxidized by a dehydrogenase to form an aldonolactone; after hydrolysis by a lactonase, the linear aldonate is dehydrated and further catabolized. Accordingly, we also attempted to grow *P. aeruginosa* in the presence of L-lyxose, D-gulose, or L-mannose; however, no growth was observed (Supporting Information, Figure 1).

The genome neighborhood of the gene encoding LyxD in *P. aeruginosa* PAO1 is shown in Figure 3; this genome context is conserved for other members of the LyxD family including the



#	UniProt	Function based on homology	Locus ID
1	Q9I1Q7	Transporter	PA2210
2	Q9I1Q6	Amidohydrolase (AH)	PA2211
3	Q9I1Q5	4-Hydroxythreonin-4-phosphate Dh (PdxA-like)	PA2212
4	Q9I1Q4	Porin	PA2213
5	Q9I1Q3	L-Lyxonate Transporter	PA2214
6	Q9I1Q2	L-Lyxonate D (LyxD)	PA2215
7	Q9I1Q1	2-Keto-3-deoxy-L-arabinonate D (L-KdID)	PA2216
8	Q9I1Q0	Semialdehyde Dh ( $\alpha$ KGSDH)	PA2217

**Figure 3.** Genome neighborhood of the gene encoding LyxD in *Pseudomonas aeruginosa* PAO1. The functions of the proteins were predicted based on the identities/functions of their closest homologues. From RT-PCR, the genes encoding LyxD and L-KdID colored in purple are cotranscribed. The transporter presumably is a L-lyxonate transporter.

**Scheme 2**

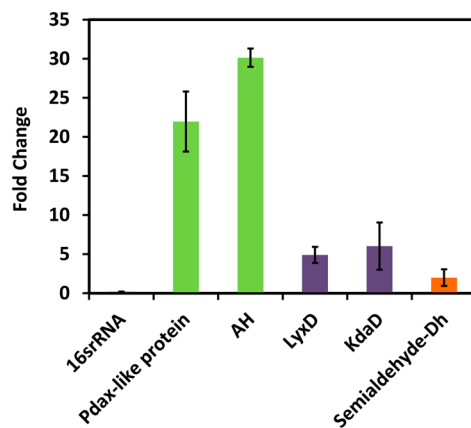
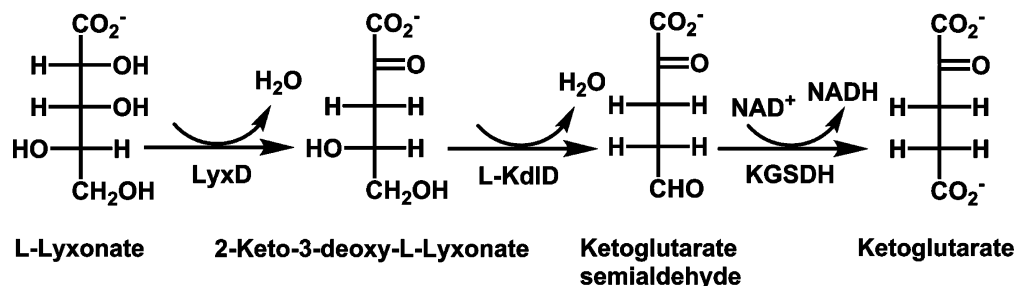


**Figure 4.** QRT-PCR results. The genes in the genome neighborhood of LyxD are upregulated 5–20-fold when the bacteria are grown on L-lyxonate (compared to D-glucose).

On the basis of the transcript analysis and the known functions of homologues of the proteins encoded by the neighboring genes (Figure 3), we proposed that the next enzyme in the catabolic pathway is L-KdI dehydratase (Scheme 2). Although L-KdI is an intermediate in the L-arabinose catabolic pathway, the dehydratase that converts L-KdI to  $\alpha$ -ketoglutarate semialdehyde in

that pathway is a member of the dihydridipicolinate synthase (DHDPS) superfamily.<sup>24</sup>

The putative L-KdI dehydratase encoded by the *P. aeruginosa* PAO1 genome is a member of the fumarylacetoacetate hydrolase (FAH) superfamily.<sup>25</sup> However, the genome neighborhoods of *Labrenzia aggregata* IAM 12614 and several other organisms that encode a LyxD lack the putative L-KdI dehydratase from the FAH family; instead, they include a gene that encodes a member of the DHDPS family that likely is the L-KdI dehydratase.

The previously characterized 2-keto-3-deoxy-D-arabinonate dehydratase (D-KdA) in the FAH superfamily utilizes Mg<sup>2+</sup> to stabilize the enolate anion intermediate.<sup>26</sup> The mechanism of the putative L-KdI dehydratase reaction in the DHDPS superfamily is expected to involve the formation of a Schiff base between the substrate and an active site Lys residue.<sup>27</sup> The kinetic constants for the FAH superfamily L-KdI dehydratases from *P. aeruginosa* PAO1 (UniProt accession ID Q9I1Q1) and *Agrobacterium tumefaciens* strain C58 (UniProt accession ID Q7CX99) and the DHDPS superfamily dehydratase from *L. aggregata* (UniProt accession ID A0NP47) were measured with a coupled enzyme assay (Table 3). The catalytic efficiencies of all three dehydratases are 10<sup>4</sup>–10<sup>5</sup> M<sup>-1</sup> s<sup>-1</sup>, so these analogous enzymes have evolved to catalyze the reaction with the same catalytic efficiencies.

**Characterization of the Pathway Enzymes:  $\alpha$ KGSDH.** The proposed function for the next enzyme in the LyxD catabolic

Table 3. Kinetic Constants for Enzymes in the L-Lyxonate Catabolic Pathway

enzyme	UniProt ID	substrate	$k_{cat}$ ( $s^{-1}$ )	$K_m$ (mM)	$k_{cat}/K_m$ ( $M^{-1} s^{-1}$ )
L-KdID-FAH	Q9I1Q1	2-keto-3-deoxy-L-lyxonate	$5 \pm 0.3$	$0.2 \pm 0.04$	$3 \times 10^4$
L-KdID-FAH	Q7CX99	2-keto-3-deoxy-L-lyxonate	$80 \pm 3$	$0.2 \pm 0.04$	$4 \times 10^5$
L-KdID-DHDPS	A0NP47	2-keto-3-deoxy-L-lyxonate	$2 \pm 0.1$	$0.07 \pm 0.01$	$3 \times 10^4$
$\alpha$ KGSDH	Q9I1Q0	$\alpha$ -ketoglutarate semialdehyde	$2 \pm 0.5$	$0.05 \pm 0.02$	$4 \times 10^5$

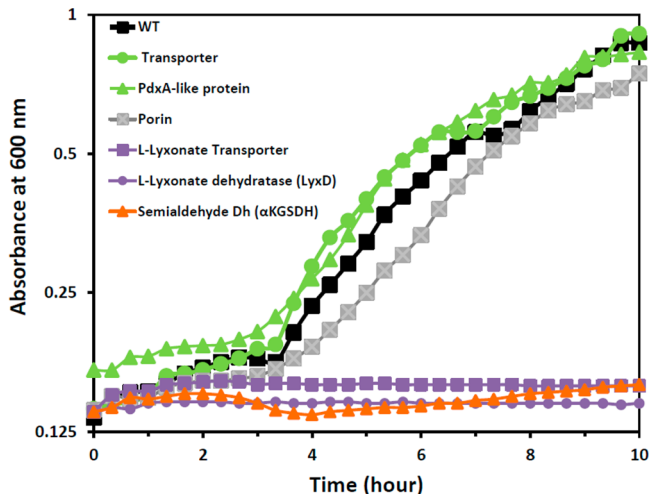


**Figure 5.** Growth phenotypes of knockouts. Knockouts of genes in *P. aeruginosa* PAO1 encoding a transporter, PdxA-like protein, porin, L-lyxonate transporter, LyxD, and  $\alpha$ KGSDH were tested for growth on L-lyxonate. Strains carrying deletions in the genes encoding the L-lyxonate transporter, LyxD, and  $\alpha$ KGSDH lost their ability to utilize L-lyxonate.

pathway (UniProt accession ID Q9I1Q0; Figure 3) is to form  $\alpha$ -ketoglutarate from  $\alpha$ -ketoglutarate semialdehyde, the product of the L-Kda/L-Kdl dehydratase (Scheme 2). The kinetic constants were determined with a spectrophotometric assay and are presented in Table 3. As predicted, this protein catalyzes the  $\alpha$ KGSDH reaction (catalytic efficiency  $10^5 M^{-1} s^{-1}$ ).

**AH and PdxA-Like Enzymes.** The genes encoding the AH and PdxA-like proteins are up-regulated in L-lyxonate grown cells (green, Figure 3); however, they are not involved in the catabolism of L-lyxonate. The substrates for these enzymes are unknown. The genome for *P. aeruginosa* PAO1 encodes an authentic PdxA protein, so the presence of this parologue suggests a new, but as of yet unknown, function for this PdxA-like protein.

**Phenotypes of Transposon-Insertion Mutants.** To further determine whether the genes in the neighborhood of that encoding LyxD were required for growth on L-lyxonate, we performed growth experiments using strains from a *P. aeruginosa* PAO1 mutant library generated by transposon-insertion mutagenesis.<sup>28</sup> Mutant strains containing disruptions in the genes encoding LyxD, the nearby transporter, and L-Kdl dehydratase (purple, Figure 3) lost the ability to grow on L-lyxonate (Figure 5). Mutant strains containing disruptions in the genes encoding the member of the AH superfamily and the PdxA-like protein retained wild type growth on L-lyxonate.

These results provide further support for not only the *in vitro* activities but also the results from the transcriptomic studies. Taken together, our *in vitro* enzymatic assays and *in vivo* physiological studies establish that LyxD, L-Kdl dehydratase, and  $\alpha$ KGSDH are responsible for the catabolism of L-lyxonate.

**X-ray Structure.** A structure for LyxD from *L. aggregata* IAM 12614 (UniProt AC A0NP48, with Mg<sup>2+</sup>, and PDB entry 3STP) was determined that showed the bidomain structure observed in other members of the enolase superfamily: an  $(\alpha + \beta)$  capping domain and a  $(\beta/\alpha)\beta$ -barrel domain. The  $\alpha + \beta$  capping domain contains residues 1–145 at the N-terminus and residues 377–390 at the C-terminus of the polypeptide; the barrel domain contains residues 146–337.

In members of the MR subgroup, the distal portion of the substrate interacts with the 20s and 50s loops in the  $(\alpha + \beta)$  capping domain, so these are important in determining substrate specificity. In LyxD, the 20s loop is long, containing residues 14–45 (Figure 6); the 50s loop is very short, containing only residues 65–66.

We were unable to obtain a liganded structure for any LyxD. The 20s loop is closed in PDB entry 3STP, so it was used as a template for *in silico* docking of L-lyxonate (Figure 6). The ligands for the required Mg<sup>2+</sup> ion are Glu 214, Glu 240, and Glu 266 located at the C-terminal ends of third, fourth, and fifth  $\beta$ -strands. As expected for a member of the MR subgroup, His316, located at the C-terminal end of the seventh  $\beta$ -strand, forms a

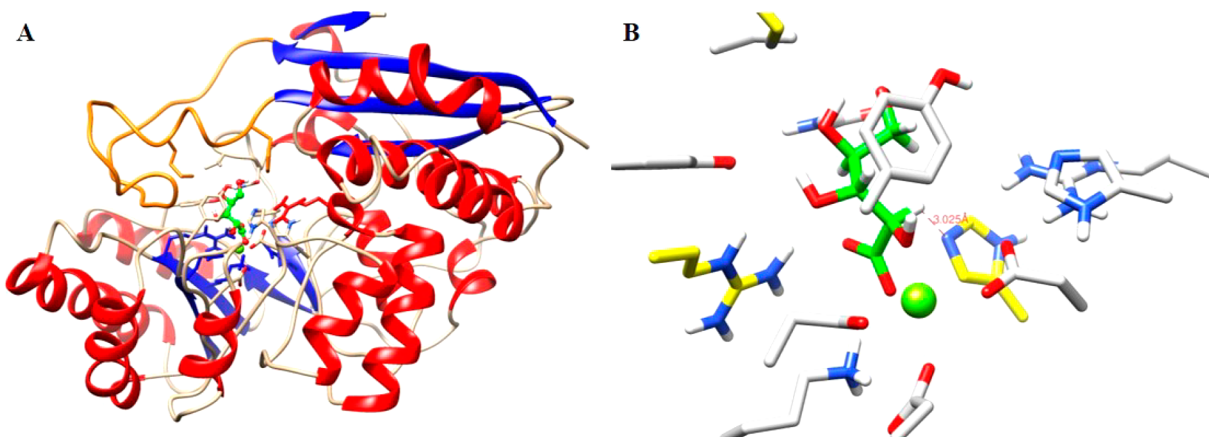


**Figure 6.** (A) Structure of LyxD from *L. aggregata* IAM 12614 (PDB: 3STP). The “20s loop” is colored orange. (B) Active site structure. The substrate is colored green, and the specificity-determining residues are colored gray. Residues in yellow are conserved catalytic residues.

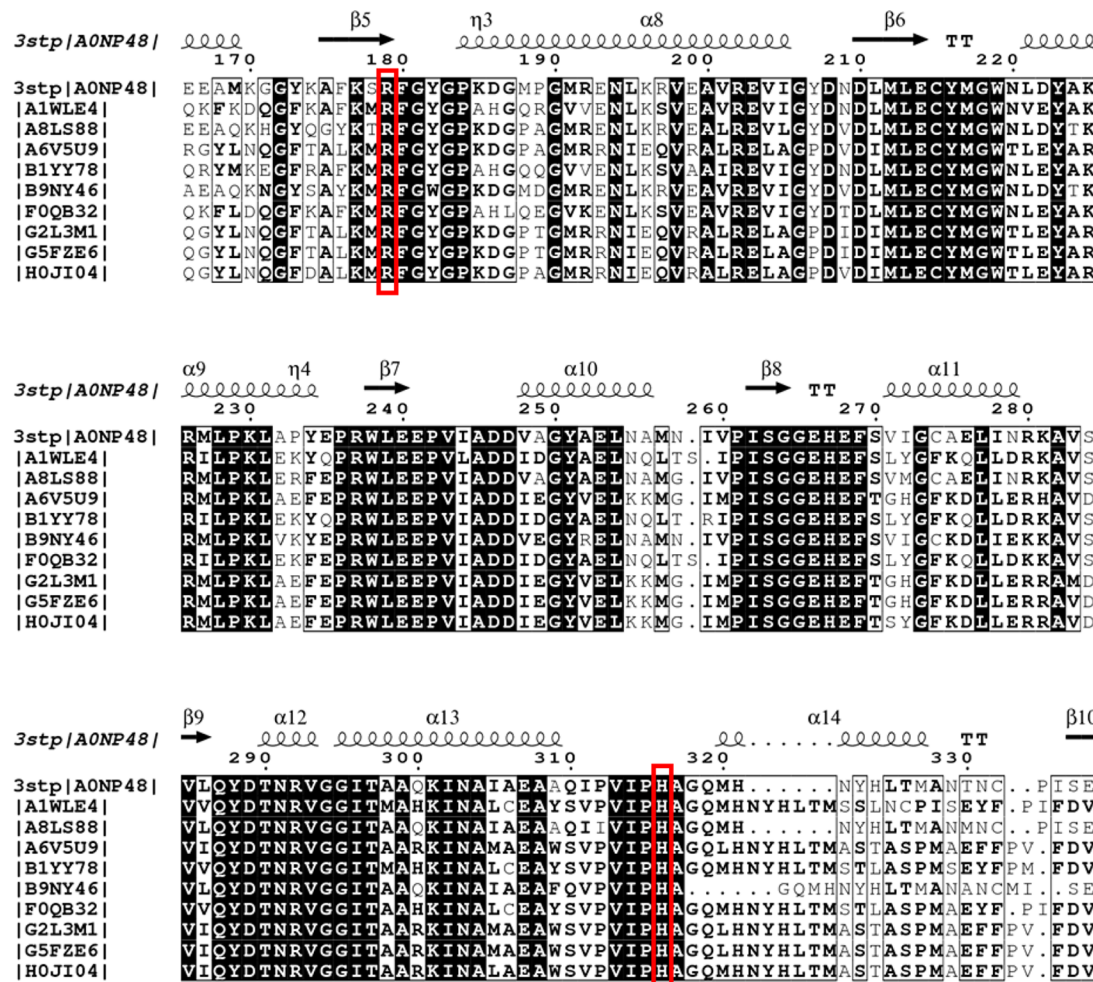


**Figure 7.** Multiple sequence alignment of LyxD orthologues. Secondary structure elements are shown on top based on the 3STP structure:  $\alpha$ -helices with squiggles,  $\beta$ -strands with arrows, and turns with TT. Conserved residues are highlighted in black. The red boxes denote the required His 316 and Arg 179 that are the conserved catalytic residues. ESPript (<http://escript.ibcp.fr>) was used to generate the alignment.

hydrogen-bonded dyad with Asp289, located at the C-terminal end of the sixth  $\beta$ -strand; together, they act as the general basic catalyst that initiates the reaction.

In other MR members, two Lys residues are located at the C-terminal end of the second  $\beta$ -strand, the first acting as an electrophile to interact with one oxygen of the substrate's carboxylate group and a second acting as an acid/base catalyst. In the LyxD family, Lys177 and Arg 179 (KxR motif) are located at the C-terminal end of the second  $\beta$ -strand.

**Site-Directed Mutagenesis.** Site-directed mutagenesis studies were performed to investigate the catalytic roles of Arg 179 and His 316 (Table 2B). The H316Q mutant had no detectable catalytic activity, as expected if His 316 is the general base that initiates the reaction. Also, the R179Q mutation also abolished LyxD activity. Mutating Arg 179 to a Lys gave rise to an insoluble protein, preventing kinetic characterization. In the vicinity of Arg 179, Tyr 216 points toward the active site; mutation to Phe did not affect the activity, suggesting that Tyr 216 has no catalytic role (Table 2B). The sequence alignment of LyxD orthologues showed that His 316 and Arg 179 are conserved (Figure 7).<sup>29</sup>

## CONCLUSIONS

Many members of the MR subgroup of the enolase superfamily are encoded by gene clusters/operons that encode proteins involved in sugar catabolism (e.g., kinases, dehydratases, dehydrogenases, and

aldolases).<sup>22</sup> The members of the previously uncharacterized cluster in Figure 1 were identified as LyxDs. Enzymatic, phenotypic, and transcriptomic data identify the catabolic pathway in which LyxD participates, the conversion of L-lyxonate to  $\alpha$ -ketoglutarate.

## ASSOCIATED CONTENT

### Supporting Information

The sequences of the primers used in qRT-PCR experiment, conserved residues in the subgroups of the enolase superfamily, and the results of growth screening of *Pseudomonas aeruginosa* PAO1 on aldoses. This material is available free of charge via the Internet at <http://pubs.acs.org>.

### Accession Codes

Model coordinates and structure factors for the LyxD from *L. aggregata* IAM 12614 with Mg<sup>2+</sup> in the active site have been deposited in the PDB (3STP). This article describes the characterization of in vitro enzymatic activities of proteins with the following UniProt accession IDs: A0NP47, A1WLE4, A8LS88, Q7CX99, Q9I1Q0, and Q9I1Q1.

## AUTHOR INFORMATION

### Corresponding Author

\*Institute for Genomic Biology, University of Illinois, 1206 W. Gregory Dr., Urbana, IL 61801. Phone: 217-244-7414. Fax: 217-333-0508. E-mail: j-gerlt@illinois.edu.

**Funding**

This research was supported by a program project grant and two cooperative agreements from the US National Institutes of Health (P01GM071790, US4GM074945, and US4GM094662).

**Notes**

The authors declare no competing financial interest.

**ACKNOWLEDGMENTS**

We thank Dr. Chakrapani Kalyanaraman, University of California, San Francisco, for docking L-lyxonate to the 3STP structure and the NIH for NIH grant P30DK089507 that provided the *P. aeruginosa* PAO1 knockout collection. Fiona P. Groninger-Poe and Jason T. Bouvier provided helpful discussions. Molecular graphics and analyses were performed with the UCSF Chimera package; Chimera is developed by the Resource for Biocomputing, Visualization, and Informatics at the University of California, San Francisco (supported by NIGMS P41-GM103311). We thank Protein Crystallography Research Resource (PXRR) of Brookhaven National Laboratory for providing data collection facilities (X29) at the National Synchrotron Light Source.

**ABBREVIATIONS**

LyxD, L-lyxonate dehydratase;  $\alpha$ KGS,  $\alpha$ -ketoglutarate semi-aldehyde;  $\alpha$ KGSDH,  $\alpha$ -ketoglutarate semialdehyde dehydrogenase; L-Kda, 2-keto-3-deoxy-L-arabinonate; L-Kdl, 2-keto-3-deoxy-L-lyxonate; DHDPS, dihydridopicolinic synthase; FAH, fumarylacetate hydrolase; MR, mandelate racemase; AraD, D-arabinonate dehydratase; FucD, L-fuconate dehydratase; GlcD, D-gluconate dehydratase; TarD, D-tartrate dehydratase; TalrD/GalrD, L-talarate/galactarate dehydratase; RhamD, L-rhamnonate dehydratase; GalD, D-galactonate dehydratase; D-KdAD, 2-keto-3-deoxy-D-arabinonate dehydratase

**REFERENCES**

- (1) Schnoes, A. M., Brown, S. D., Dodevski, I., and Babbitt, P. C. (2009) Annotation error in public databases: misannotation of molecular function in enzyme superfamilies. *PLoS Comp. Biol.* 5, e1000605.
- (2) Lukk, T., Sakai, A., Kalyanaraman, C., Brown, S. D., Imker, H. J., Song, L., Fedorov, A. A., Fedorov, E. V., Toro, R., Hillerich, B., Seidel, R., Patkovsky, Y., Vetting, M. W., Nair, S. K., Babbitt, P. C., Almo, S. C., Gerlt, J. A., and Jacobson, M. P. (2012) Homology models guide discovery of diverse enzyme specificities among dipeptide epimerases in the enolase superfamily. *Proc. Natl. Acad. Sci. U.S.A.* 109, 4122–4127.
- (3) Yew, W. S., Fedorov, A. A., Fedorov, E. V., Rakus, J. F., Pierce, R. W., Almo, S. C., and Gerlt, J. A. (2006) Evolution of enzymatic activities in the enolase superfamily: L-fuconate dehydratase from *Xanthomonas campestris*. *Biochemistry* 45, 14582–14597.
- (4) Hubbard, B. K., Koch, M., Palmer, D. R., Babbitt, P. C., and Gerlt, J. A. (1998) Evolution of enzymatic activities in the enolase superfamily: characterization of the (D)-glucarate/galactarate catabolic pathway in *Escherichia coli*. *Biochemistry* 37, 14369–14375.
- (5) Gerlt, J. A., Babbitt, P. C., Jacobson, M. P., and Almo, S. C. (2012) Divergent evolution in enolase superfamily: strategies for assigning functions. *J. Biol. Chem.* 287, 29–34.
- (6) Gerlt, J. A., Babbitt, P. C., and Rayment, I. (2005) Divergent evolution in the enolase superfamily: the interplay of mechanism and specificity. *Arch. Biochem. Biophys.* 433, 59–70.
- (7) Savitsky, P., Bray, J., Cooper, C. D., Marsden, B. D., Mahajan, P., Burgess-Brown, N. A., and Gileadi, O. (2010) High-throughput production of human proteins for crystallization: the SGC experience. *J. Struct. Biol.* 172, 3–13.
- (8) Studier, F. W. (2005) Protein production by auto-induction in high density shaking cultures. *Protein Expression Purif.* 41, 207–234.
- (9) Ho, S. N., Hunt, H. D., Horton, R. M., Pullen, J. K., and Pease, L. R. (1989) Site-directed mutagenesis by overlap extension using the polymerase chain reaction. *Gene* 77, 51–59.
- (10) Livak, K. J., and Schmittgen, T. D. (2001) Analysis of relative gene expression data using real-time quantitative PCR and the 2(-Delta Delta C(T)) Method. *Methods* 25, 402–408.
- (11) Otwinowski, Z., and Minor, W. (1997) Processing of X-ray diffraction data collected in oscillation mode. *Methods Enzymol.* 276, 307–326.
- (12) Vagin, A., and Teplyakov, A. (2010) Molecular replacement with MOLREP. *Acta Crystallogr., Sect. D* 66, 22–25.
- (13) Perrakis, A., Morris, R., and Lamzin, V. S. (1999) Automated protein model building combined with iterative structure refinement. *Nat. Struct. Biol.* 6, 458–463.
- (14) Brunger, A. T., Adams, P. D., Clore, G. M., DeLano, W. L., Gros, P., Grosse-Kunstleve, R. W., Jiang, J. S., Kuszewski, J., Nilges, M., Pannu, N. S., Read, R. J., Rice, L. M., Simonson, T., and Warren, G. L. (1998) Crystallography & NMR system: A new software suite for macromolecular structure determination. *Acta Crystallogr., Sect. D* 54, 905–921.
- (15) Emsley, P., Lohkamp, B., Scott, W. G., and Cowtan, K. (2010) Features and development of Coot. *Acta Crystallogr., Sect. D* 66, 486–501.
- (16) Rakus, J. F., Fedorov, A. A., Fedorov, E. V., Glasner, M. E., Hubbard, B. K., Delli, J. D., Babbitt, P. C., Almo, S. C., and Gerlt, J. A. (2008) Evolution of enzymatic activities in the enolase superfamily: L-rhamnonate dehydratase. *Biochemistry* 47, 9944–9954.
- (17) Brouns, S. J., Walther, J., Snijders, A. P., van de Werken, H. J., Willemen, H. L., Worm, P., de Vos, M. G., Andersson, A., Lundgren, M., Mazon, H. F., van den Heuvel, R. H., Nilsson, P., Salmon, L., de Vos, W. M., Wright, P. C., Bernander, R., and van der Oost, J. (2006) Identification of the missing links in prokaryotic pentose oxidation pathways: evidence for enzyme recruitment. *J. Biol. Chem.* 281, 27378–27388.
- (18) Wieczorek, S. W., Kalivoda, K. A., Clifton, J. G., Ringe, D., Petsko, G. A., and Gerlt, J. A. (1999) Evolution of enzymatic activities in the enolase superfamily: Identification of a new general acid catalyst in the active site of D-galactonate dehydratase from *Escherichia coli*. *J. Am. Chem. Soc.* 121, 4540–4541.
- (19) Yew, W. S., Fedorov, A. A., Fedorov, E. V., Wood, B. M., Almo, S. C., and Gerlt, J. A. (2006) Evolution of enzymatic activities in the enolase superfamily: D-tartrate dehydratase from *Bradyrhizobium japonicum*. *Biochemistry* 45, 14598–14608.
- (20) Ahmed, H., Ettema, T. J., Tjaden, B., Geerling, A. C., van der Oost, J., and Siebers, B. (2005) The semi-phosphorylative Entner-Doudoroff pathway in hyperthermophilic archaea: a re-evaluation. *Biochem. J.* 390, 529–540.
- (21) Lamble, H. J., Milburn, C. C., Taylor, G. L., Hough, D. W., and Danson, M. J. (2004) Gluconate dehydratase from the promiscuous Entner-Doudoroff pathway in *Sulfolobus solfataricus*. *FEBS Lett.* 576, 133–136.
- (22) Yew, W. S., Fedorov, A. A., Fedorov, E. V., Almo, S. C., and Gerlt, J. A. (2007) Evolution of enzymatic activities in the enolase superfamily: L-talarate/galactarate dehydratase from *Salmonella typhimurium* LT2. *Biochemistry* 46, 9564–9577.
- (23) Kuorelahti, S., Jouhten, P., Maaheimo, H., Penttila, M., and Richard, P. (2006) L-galactonate dehydratase is part of the fungal path for D-galacturonic acid catabolism. *Mol. Microbiol.* 61, 1060–1068.
- (24) Watanabe, S., Shimada, N., Tajima, K., Kodaki, T., and Makino, K. (2006) Identification and characterization of L-arabonate dehydratase, L-2-keto-3-deoxyarabonate dehydratase, and L-arabinolactonase involved in an alternative pathway of L-arabinose metabolism. Novel evolutionary insight into sugar metabolism. *J. Biol. Chem.* 281, 33521–33536.
- (25) Watanabe, S., Shimada, N., Tajima, K., Kodaki, T., and Makino, K. (2006) Identification and characterization of L-arabonate dehydratase, L-2-keto-3-deoxyarabonate dehydratase, and L-arabinolactonase involved in an alternative pathway of L-arabinose metabolism. Novel

evolutionary insight into sugar metabolism. *J. Biol. Chem.* 281, 33521–33536.

(26) Brouns, S. J., Barends, T. R., Worm, P., Akerboom, J., Turnbull, A. P., Salmon, L., and van der Oost, J. (2008) Structural insight into substrate binding and catalysis of a novel 2-keto-3-deoxy-D-arabinonate dehydratase illustrates common mechanistic features of the FAH superfamily. *J. Mol. Biol.* 379, 357–371.

(27) Stoolmiller, A. C., and Abeles, R. H. (1966) Formation of alpha-ketoglutaric semialdehyde from L-2-keto-3-deoxyarabonic acid and isolation of L-2-keto-3-deoxyarabonate dehydratase from *Pseudomonas saccharophila*. *J. Biol. Chem.* 241, 5764–5771.

(28) Jacobs, M. A., Alwood, A., Thaipisuttikul, I., Spencer, D., Haugen, E., Ernst, S., Will, O., Kaul, R., Raymond, C., Levy, R., Chun-Rong, L., Guenther, D., Bovee, D., Olson, M. V., and Manoil, C. (2003) Comprehensive transposon mutant library of *Pseudomonas aeruginosa*. *Proc. Natl. Acad. Sci. U.S.A.* 100, 14339–14344.

(29) Gouet, P., Robert, X., and Courcelle, E. (2003) ESPript/ENDscript: Extracting and rendering sequence and 3D information from atomic structures of proteins. *Nucleic Acids Res.* 31, 3320–3323.